INTERNATIONAL JOURNAL OF
ENERGY AND ENVIRONMENT

Volume 7, Issue 4, 2016 pp.317-326
Journal homepage: www.IJEE.IEEFoundation.org

Investigation potential flow about swept back wing using panel method

Wakkas Ali Rasheed, Nabeel Abdulhadi Ghyadh, Sahib Shihab Ahmed

Department of Mechanical Engineering, Faculty of Engineering, Al-Kufa University, Ministry of Higher Education & Scientific Research, Iraq.

Abstract
In the present investigation Low order panel method with Dirichlet boundary condition conjugated with Kutta condition, was used to calculate pressure coefficients for potential flow about isolated swept back wings at different aspect ratios and different angles of attack. Also both local and total lift coefficients were calculated for the same wings, with detailed streamline behavior on both upper and lower surface. Constant strength quadrilateral doublet element and Constant strength quadrilateral source element were placed on each panel, except on wake sheet only constant strength quadrilateral doublets were placed to satisfy Kutta condition at trailing edge. A set of linear algebraic equations were established by setting inner potential equals to free stream potential. These equations were solved using Gauss-elimination to determine quadrilateral doublet singularity strength distribution. Finally finite difference formula was used to predict aerodynamic loads calculation.

Keywords: Panel method; Potential flow; Swept back wing; Lift coefficients.

1. Introduction

The interference problem among the components of an airplane or missile has received extensive attention because of its importance in modern airplane design. This importance is due to the interest in designs employing small wing to tail span [1]. The reason for the use of swept wings in the design of aircraft for high subsonic speeds is due to that a swept wing has a greater critical Mach number above which the drag may rise sharply than a corresponding unswept wing [2]. It is not appropriate in modern aircraft design to ignore the influences of the static structural deformation on flight loads, static stability, controlling derivatives and other flight performance. Therefore, analysis for pressure distribution is very important for its considering deformation effect. Accurate predictions of static aeroelastic characteristics, which are especially important in the early design stage of aircraft, can be used to avoid revising the structural design repeatedly in the late phase of aircraft design. Many efforts [3].Have been made to develop accurate and suitable methods to predict aerodynamic loads. Panel method has been widely accepted as a useful tool for aerodynamic and hydrodynamic design, since it's has been developed by Hess and Smith [4]. A large number of different panel methods have been developed for a variety of applications, leading recently to application to the analysis of steady performance [5]. One of the earliest attempts to study and employ such methods is the work of K.ICHEMANN and J. WEBER [2] have been given a review was of the effects associated with the subsonic inviscid flow past swept wings at zero lift

with the aim of providing the information needed for an understanding of the flow phenomena, methods of obtaining the full benefit of sweep were described.

Raad Shehab Ahmed [6] has studied the transonic flow past unswept and swept wings. The velocity field and pressure coefficients were estimated as function of free stream Mach number. The results show the effect of free stream Mach number on shock waves location and the velocity field around the wing section. The Euler solution and potential flow solutions were identical at subsonic flow; however, at supersonic flow the potential theory can no longer predict the flow field correctly. The results show the important effect of sweep angle on the value of the critical Mach number for wings.

G.K.Ananda et al. [7] have studied the low Reynolds number aerodynamics of ten wings having aspect ratios ranging from 2 to 5. In this low-to-moderate aspect ratio range, yet this range spans that of many typical modern small-scale UAVs that operate in the 50,000 to 150,000 Reynolds number range. Both straight and tapered wings were wind tunnel tested, and flow visualization was performed to characterize the flow. The measurements showed that all wings exhibited sensitivity to changes in aspect ratio and Reynolds number. Oswald's efficiency factors derived from the measurements ranged from a low value of 0.3 to more typical values near 0.8. Additionally, the aerodynamic performance trends relating to the maximum lift coefficient, lift curve slope.

A.R. Davari et al. [1] have done an extensive wind tunnel tests on several wing- body-tail combinations in subsonic flow to study the effects of wing geometric parameters on the flow field over the tail. For each configuration, tail surface pressure distribution, as well as the velocity contour at a plane perpendicular to the flow direction behind the wing was measured. The results show a strong effect of wing to tail span ratio, as well as wing aspect ratio, on the flow field downstream of the wing. For low sweep wings, as those considered here, wing and body interference effects on the tail are associated with the wing tip vortex and nose-body vortex.

P.O. Persson et al. [8] have simulated numerically a set of flapping wing problems using both a low-order potential flow model and a high-order accurate Navier-Stokes solver. The simulations confirm the challenges in analyzing and designing effective flapping wings. Potential flow method predicts accurate results for attached flow cases. It is critical to accompany any inviscid design predictions with a viscous simulation to confirm the predicted behavior.

NACA 0012 was used in our study to investigates pressure coefficient distribution, local lift coefficient distribution, velocity to free stream velocity ratio distribution on both upper and lower surfaces and lift coefficient for wing with difference sweep back angles (0,20,30,40,50 and 60) and different aspect ratios (2,3,4 and 5). For each case different angle of attack was studied to draw total lift coefficient behaviour within range of (0-12) degree.

2. Theoretical analyses

One of most used method for computing flow about arbitrary geometries are those which represent the configuration boundary with some form of source / doublet – vorticity distribution generally called panel method. This method was introduced by Hess and smith, the most significant capability offered by panel method is the treatment of complicated, multi-component geometries without any need for grid generation in the domain surrounding the configuration.

The panel method solvers considers potential flow (incompressible, irrational, invicid flow) only, so this method less accurate than other CFD solvers, but within the limiting theoretical assumptions, panel method solvers have provided results that are found to be in excellent agreement with test data and other data obtained by other CFD solvers. The most significant property of potential function is principal of super position. If each of Φ_1 , Φ_2 , …… , Φ_n be an equation satisfies Laplace equation which is:

$$\nabla^2 \Phi = 0 \tag{1}$$

Then the some of these equations satisfies the Laplace equation. This can be written as:

$$\Phi = \sum_{k=1}^{n} c_k \Phi_k \tag{2}$$

where C1, C_2, ……, C_m are arbitrary constants, and therefore:

$$\nabla^2 \Phi = \sum_{k=1}^{m} c_k \nabla^2 \Phi_k = 0 \tag{3}$$

Due to this property panel method can solve problems of multi-components configuration. Shape and singularity of panels determine the order of panel method. If panel surface is not linear or singularity strength distribution not linear then it's called higher order panel method else it's called low order panel method.
Consider a body with known boundaries S_B, Submerged in a potential flow. The flow in outer region is incompressible and irrotational, so continuity equation in terms of total potential function is

$$\nabla^2 \Phi^* = 0 \tag{4}$$

The general form of equation (3) can be written for a sum of sources and doublets singularities placed on solid boundary S_B of flying object, using principle of superposition the total potential function is the sum of these singularities effect with free stream effect.

$$\Phi^*(x,y,z) = -\frac{1}{4\pi}\int_{S_B}\left[\sigma\left(\frac{1}{r}\right) - \mu\, n.\nabla\left(\frac{1}{r}\right)\right] ds + \Phi_\infty \tag{5}$$

Here the normal vector n points inside the body, and Φ_∞ is the free- stream potential:
Doublets & Sources singularities used to represent non-zero thickness bodies only, while doublets only used for zero thickness bodies and so eq. (3) can be rewritten as [9].

$$\Phi^* = \frac{1}{4\pi}\int_{body+wake}\mu\, n.\nabla\left(\frac{1}{r}\right) ds - \frac{1}{4\pi}\int_{body}\sigma\left(\frac{1}{r}\right) ds + \Phi_\infty \tag{6}$$

3. Boundary conditions

3.1 Far field condition

At very far region from the body boundary the velocity must equal to free stream velocity i.e.

$$\lim_{r\to\infty} \nabla\Phi = 0 \tag{7}$$

where $= \sqrt{x^2 + y^2 + z^2}$, in potential flow this condition automatically satisfied.

3.2 Tangency condition

This condition means that normal velocity on the body surface must equal zero, two approaches may be applied to satisfy this condition which are Neumann and Dirichlet Boundary condition.

3.2.1 Dirichlet boundary condition

This condition based on setting the total potential function everywhere on solid boundaries to be constant; consequently velocity component normal to solid boundary will be zero. This condition also named indirect condition

$$\Phi^*(x,y,z)|_{S_B} = constant \tag{8}$$

In case of source / doublet distribution, this condition can be satisfied by setting ($\Phi^*_{inner} = \Phi\infty$) i.e. Inner perturbation potential equal zero.

$$\frac{1}{4\pi}\int_{body}\mu\,\frac{\partial}{\partial n}\left(\frac{1}{r}\right) ds - \frac{1}{4\pi}\int_{body}\sigma\left(\frac{1}{r}\right) ds = 0 \tag{9}$$

Sources strengths are determined by the following equation.

$$\sigma = \vec{n}\,.\,\vec{Q}_\infty \tag{10}$$

3.3 Kutta condition

This condition states that circulation of flow at trailing edge equal zero. This condition can be satisfied when each upper and lower velocity at trailing each is equaled and parallel.

$$\gamma_{trailing\ edge} = 0 \tag{11}$$

3.4 Panel method methodology

Since the integrations mentioned above cannot determined exactly, it must be determined numerically. The main steps in panel method can be summarized as follows:-

1. Grid generation, which means mainly discretization on flying body surfaces to set of panels, determining collocation points (centroid) and constructing normal vectors for each panel.
2. Placing quadrilateral source and quadrilateral doublet on each panel. Strength of source can be calculated from eq. (10), while doublets strength assumed to be unit.
3. Constructing the influence coefficient matrix [$\mathbf{a_{ij}}$] where $\mathbf{a_{ij}}$ is the normal velocity on solid boundary induced by **j** doublet at collocation point of panel **i**.
4. Constructing the RHS (right hand side) vector where RHS_i represents the sum of velocities induced by sources and free stream velocity on collocation point of panel **i**.
5. Solve the algebraic equation to yields doublet's strength:

$$[a_{ij}]\begin{bmatrix} M_1 \\ \vdots \\ M_n \end{bmatrix}=\begin{bmatrix} RHS_1 \\ \vdots \\ RHS_n \end{bmatrix} \tag{12}$$

6. Velocity can be calculated at any point by sum of induced velocities by all sources, doublets and free stream compute.

4. Results and discussion

A Fortran program was constructed by authors to perform panel method steps, on swept back wing. This section is devoted to present and discuss various numerical data obtained from implementation of this program. All contours were drawn with Tec plot 360 while all charts drawn with excel 2010 program.

Grids of 2160 panel was used on wing surfaces with full cosine discretization formula in both chord and span directions and make panel of 300 time chord at trailing edges panels. It should be mentioned that drag coefficient not included in this work because of neglecting viscous effect in potential flow, which is the main component of drag. While lift coefficient depends mainly on pressure distribution over the flying body, so this method can be used to estimate lift coefficient effectively.

Figures (1&2) illustrate pressure coefficient contours on both upper and lower surfaces for wing with (ASR=2, SBA=20 and AOAT=0) and (ASR=4, SBA=20 and AOAT=0) respectively, it can be noticed that there is symmetric behaviors in pressure coefficient distribution for both upper and lower surfaces; also there is symmetric behaviors about root chord axis. This behavior gives good verification for numerical accuracy of present work.

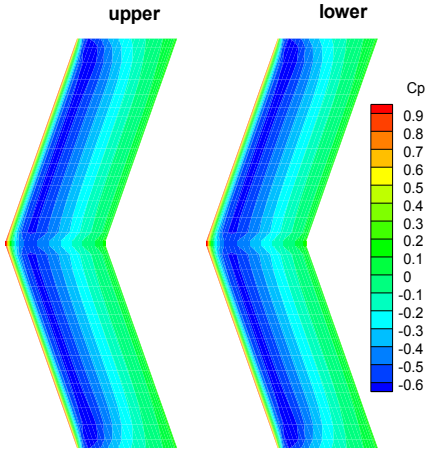

Figure 1. Pressure coefficient contours on upper and lower surfaces at (ASR=2, SBA=20& AOAT=0).

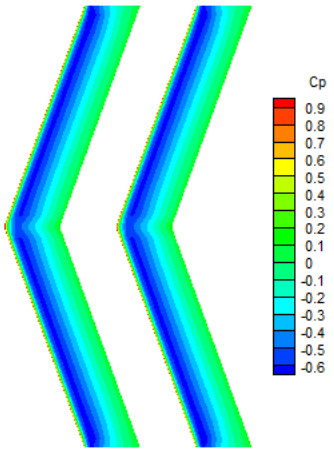

Figure 2. Pressure coefficient contours on upper and lower surfaces at (ASR=4, SBA=20& AOAT=0).

Figures (3-6) show pressure coefficient contours on both upper and lower surfaces for wing with (ASR=2,SBA=30 and AOAT=5), (ASR=2,SBA=50 and AOAT=10), (ASR=4,SBA=30 and AOAT=5) and (ASR=4,SBA=50 and AOAT=10) respectively, it can be seen there is no a symmetry for both upper and lower surfaces due to non-zero angle of attack, while symmetry about root chord axis still exists due geometrical symmetry. Pressure coefficient values on lower surface are greater than upper values specially near the leading edge due to stagnation point occurring in lower surface. At wing tips there is little change in pressure coefficient distribution behavior caused by trailing vortex formation effect.

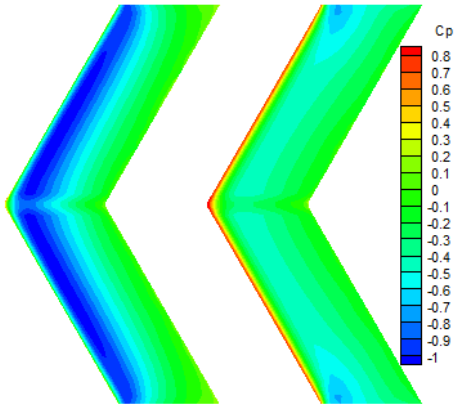

Figure 3. Pressure coefficient contours on upper and lower surfaces at (ASR=2, SBA=30& AOAT=5).

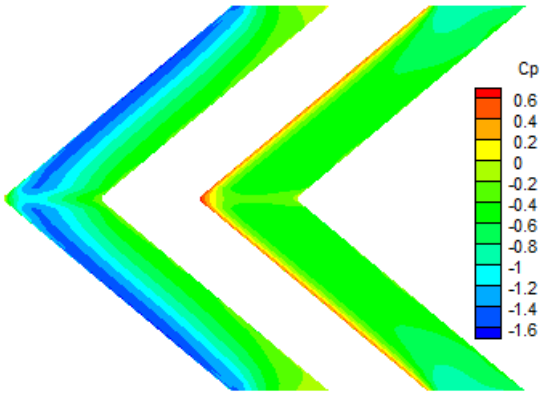

Figure 4. Pressure coefficient contours on upper and lower surfaces at (ASR=2, SBA=50& AOAT=10).

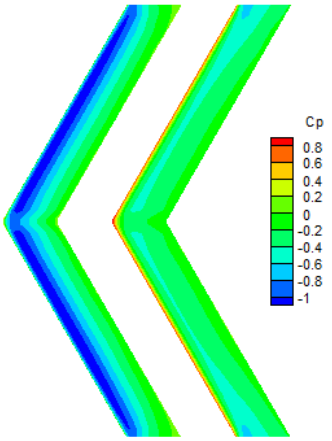

Figure 5. Pressure coefficient contours on upper and lower surfaces at (ASR=4, SBA=30& AOAT=5).

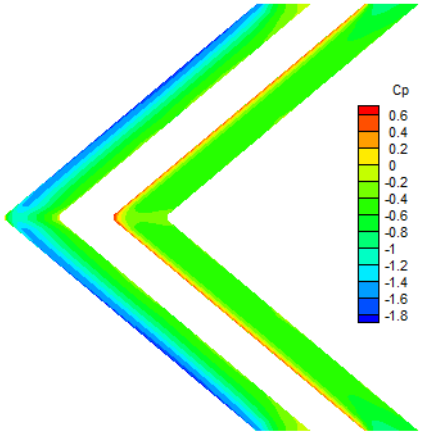

Figure 6. Pressure coefficient contours on upper and lower surfaces at (ASR=4, SBA=50& AOAT=10).

Figures (7&8) show local lift coefficient contours on both upper and lower surfaces for wing with (ASR=2, SBA=20 and AOAT=0), (ASR=4, SBA=20 and AOAT=0), respectively.

Figures (9-12) depict local lift coefficient contours on both upper and lower surfaces for wing with (ASR=2, SBA=30 and AOAT=5), (ASR=2, SBA=50 and AOAT=10), (ASR=4, SBA=30 and AOAT=5) and (ASR=4, SBA=50 and AOAT=10) respectively, the difference between upper and lower surfaces is due to different of normal vectors direction. The un symmetric results because of the presence of the angle of attack.

Figures (13-18) show velocity to free stream velocity ratio distribution contour on both upper and lower surfaces wing with (ASR=2, SBA=20 and AOAT=0), (ASR=2, SBA=30 and AOAT=5), (ASR=2, SBA=50 and AOAT=10), (ASR=4, SBA=20 and AOAT=0), (ASR=4, SBA=30 and AOAT=5) and (ASR=4, SBA=50 and AOAT=10) respectively, show formation of lateral velocity component directed away from root chord axis due to sweeping back angle.

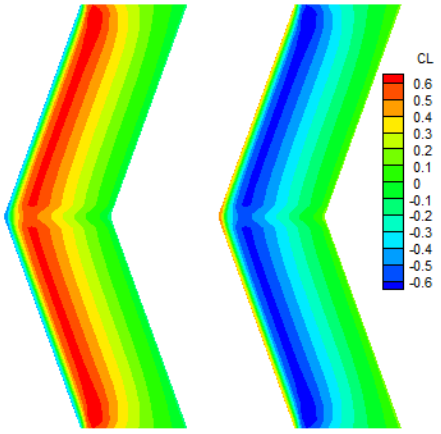

Figure 7. Local lift coefficient contours on upper and lower surfaces at (ASR=2, SBA=20& ΔOAT=0).

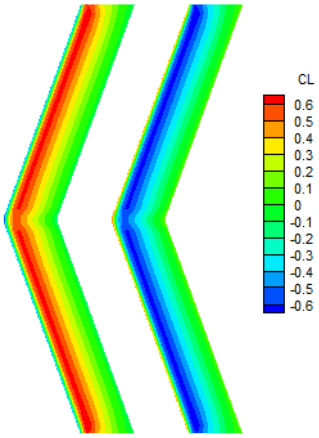

Figure 8. Local lift coefficient contours on upper and lower surfaces at (ASR=4, SBA=20& ΔOAT=0).

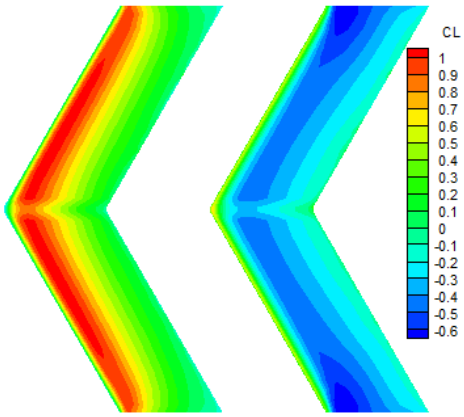

Figure 9. Local lift coefficient contours on upper and lower surfaces at (ASR=2, SBA=30& ΔOAT=5).

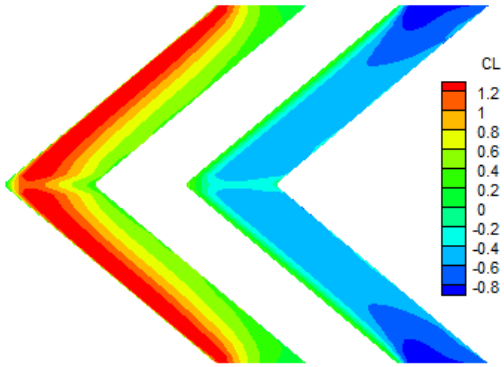

Figure 10. Local lift coefficient contours on upper and lower surfaces at (ASR=2, SBA=50& ΔOAT=10).

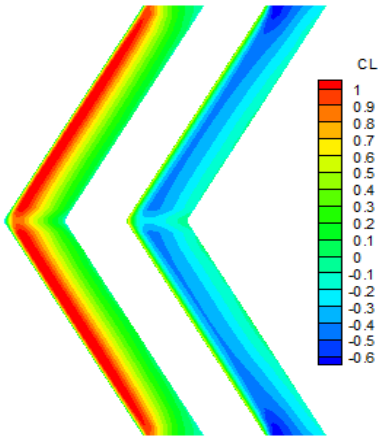

Figure 11. Local lift coefficient contours on upper and lower surfaces at (ASR=4, SBA=30& ΔOAT=5).

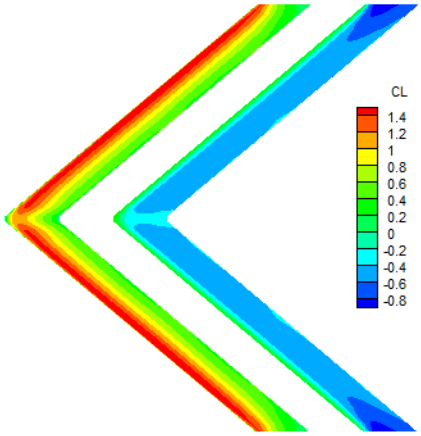

Figure 12. Local lift coefficient contours on upper and lower surfaces at (ASR=4, SBA=50& ΔOAT=10).

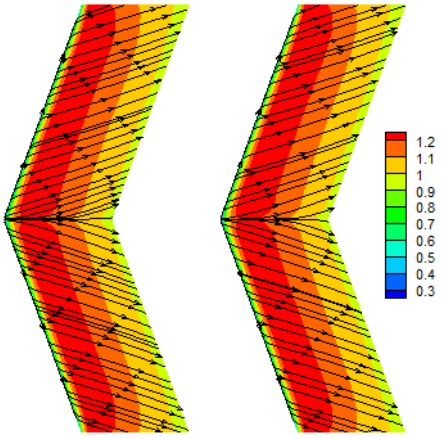

Figure 13. Stream lines behaviors & v/v_∞ contours on upper and lower surfaces (ASR=2, SBA=20& AOAT=0).

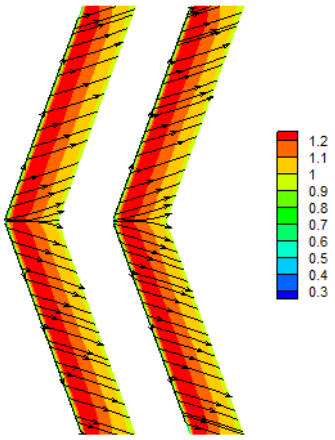

Figure 14. Stream lines behaviors & v/v_∞ contours on upper and lower surfaces (ASR=4, SBA=20& AOAT=0).

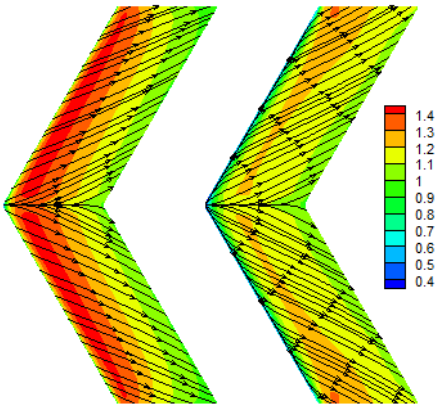

Figure 15. Stream lines behaviors & v/v_∞ contours on upper and lower surfaces (ASR=2, SBA=30& AOAT=5).

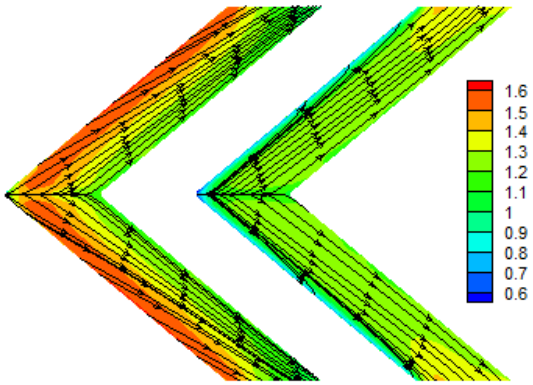

Figure 16. Stream lines behaviors & v/v_∞ contours on upper and lower surfaces (ASR=2, SBA=50& AOAT=10).

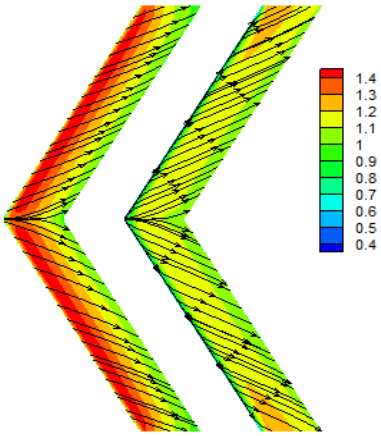

Figure 17. Stream lines behaviors & v/v_∞ contours on upper and lower surfaces (ASR=4, SBA=30& AOAT=5).

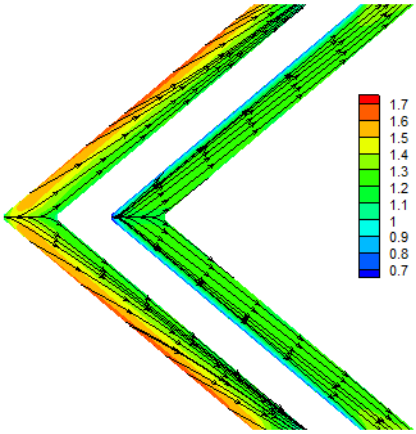

Figure 18. Stream lines behaviors & v/v_∞ contours on upper and lower surfaces (ASR=4, SBA=50& AOAT=10).

Figures (19-24) show that lift coefficient increases with angle of attack because of symmetric profile of wing used (NACA 0012), also its obvious that when sweep back angle maintained constant the lift coefficient increases with increase in aspect ratio for same angle of attack because the decreases in ratio of area that endures trailing vortex at wing tips to total area of wing. As sweep back angle increases the

difference in lift coefficient values at different aspect ratios decreases this may be due to of increase in lateral velocity induced values.

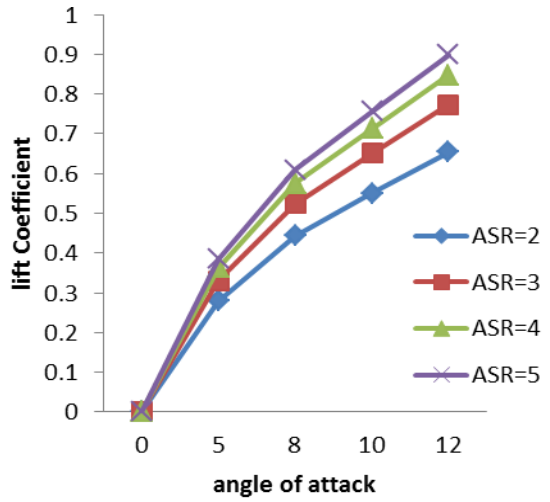

Figure 19. Lift coefficient vs. angle of attack for different aspect ratio at zero swept back angle.

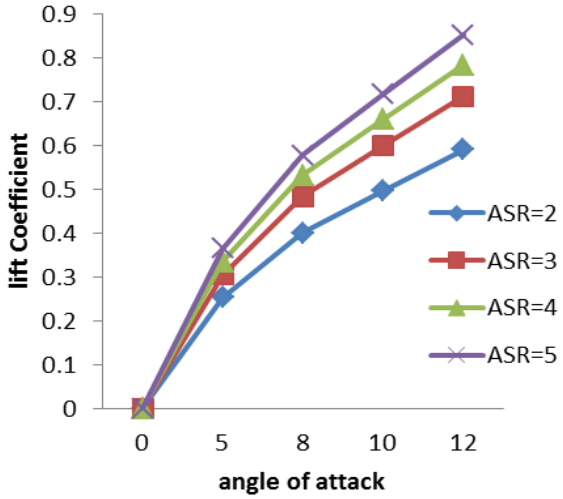

Figure20. Lift coefficient vs. angle of attack for different aspect ratio at SBA=20.

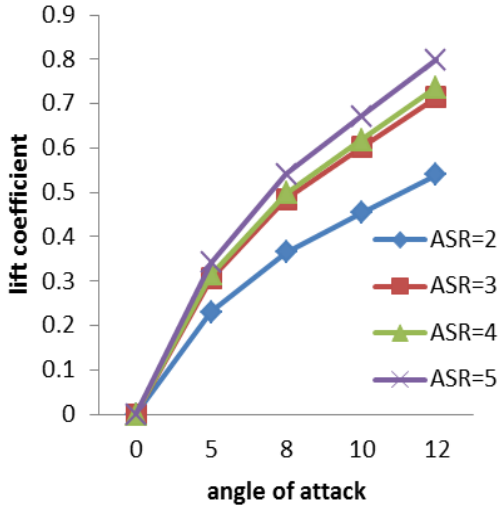

Figure 21. Lift coefficient vs. angle of attack for different aspect ratio at SBA=30.

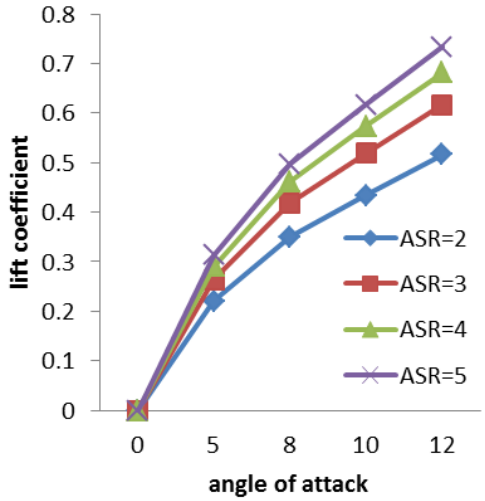

Figure 22. Lift coefficient vs. angle of attack for different aspect ratio at SBA=40.

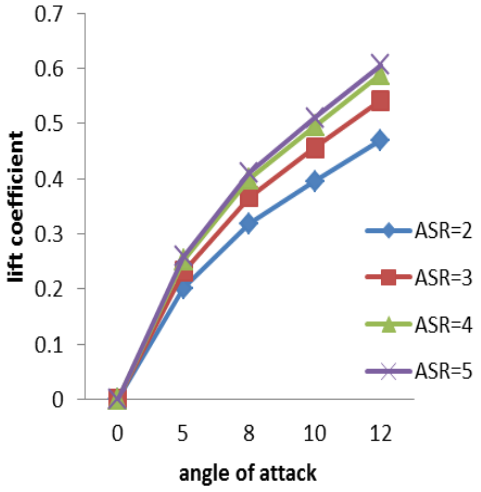

Figure 23. Lift coefficient vs. angle of attack for different aspect ratio at SBA=50.

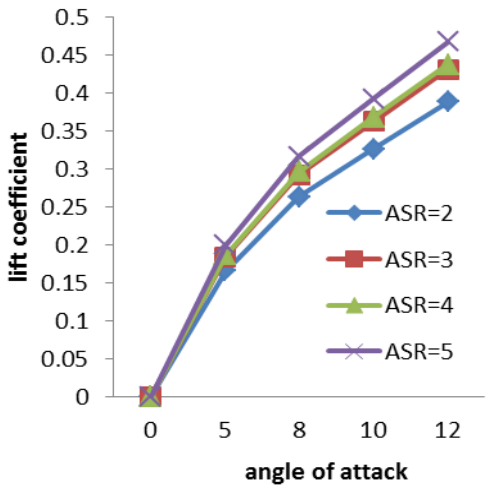

Figure 24. Lift coefficient vs. angle of attack for different aspect ratio at SBA=60.

Figures (25-28) show the decrease of lift coefficient as sweep back angle increases this due to increases in lateral velocity formation on wing.

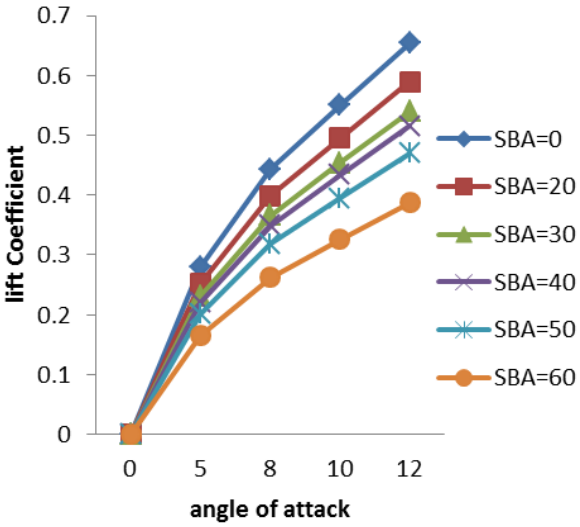

Figure 25. Lift coefficient vs. angle of attack for different swept back angle at ASR=2.

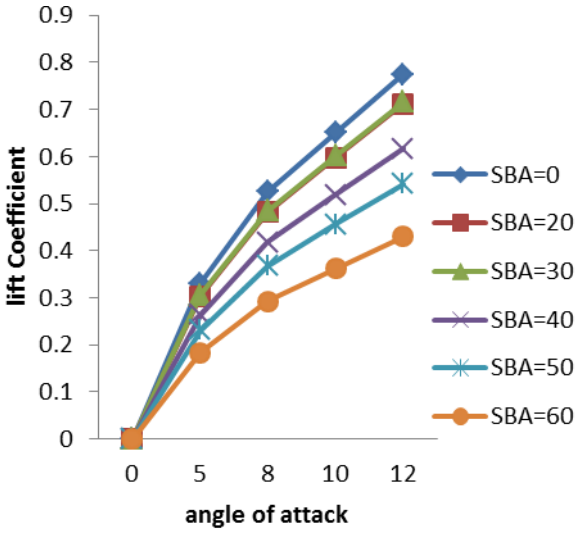

Figure 26. Lift coefficient vs. angle of attack for different swept back angle at ASR=3.

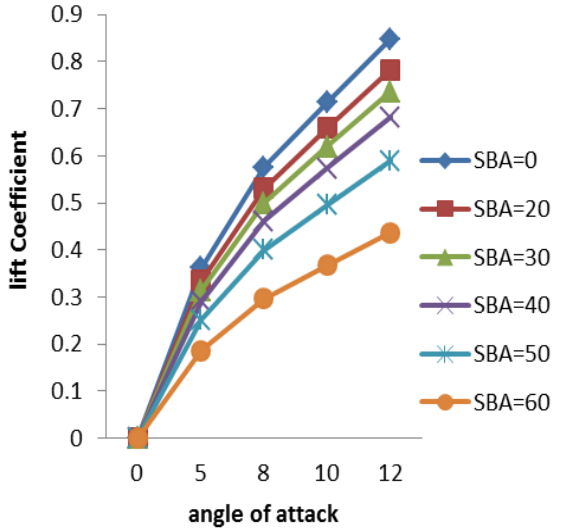

Figure 27. Lift coefficient vs. angle of attack for different swept back angle at ASR=4.

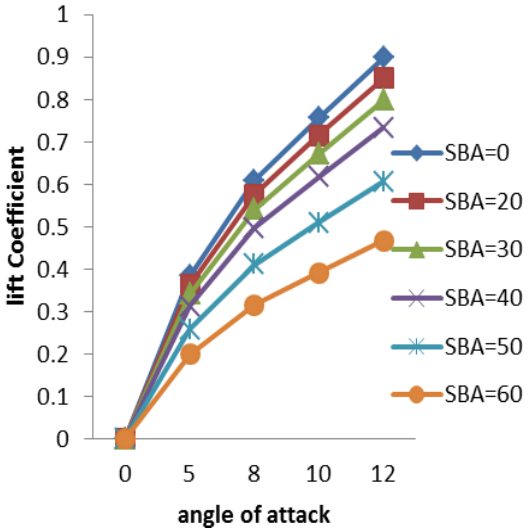

Figure 28. Lift coefficient vs. angle of attack for different swept back angle at ASR=5.

5. Conclusion

This work presents the simulated flow about swept back wing and it was observed that the lift coefficient increases aspect ratio increases because of reduction ratio of area effected with trialing vortex to total wing area. Lift coefficient decreases as sweep back angle increases due increase in lateral velocity induced directed away from root chord axis.

Nomenclature

AOAT	Angle of attack (Degree)	Φ^*	Total velocity potential function m^2/s
ASR	Aspect ratio	Φ	Velocity potential function m^2/s
SBA	Swept back angle (Degree)	Φ_∞	Free stream velocity potential function m^2/s
C_l	Left coefficient	γ	Vorticity strength m/s
C_p	Pressure coefficient	α	Angle of attack (Degree)

n	Normal unit vector	ρ	Density Kg/m^3
S_B	Solid body boundary	σ	Source strength m/s
Q	Velocity vector m/s	μ	Doublet strength m/s
Q_∞	Free stream velocity m/s		

References

[1] A.R. Davari A., M.R. Soltani B., F. Askari B. and H.R. Pajuhandea. Effects of wing geometry on wing-body-tail interference in subsonic flow. Scientia Iranica B, 2011, 18(3), 407-415.

[2] K.ICHEMANN and J. WEBER. The Subsonic Flow Past Swept Wings at Zero Lift Without and With Body. AERONAUTICAL RESEARCH COUNCIL REPORTS AND MEMORANDA, 1956, No. 2908.

[3] Yaokun Wanga, Zhiqiang Wana and Chao Yanga. Application of High-order Panel Method in Static Aero elastic Analysis of Aircraft. Procedia Engineering, 2012, 31, 136-144.

[4] Hess, J.L., Smith A.M.O. Calculation of nonlifting potential flow about arbitrary three-dimensional bodies. Journal of Ship Research, 1964, (2), 22-44.

[5] G. D. Kima, C. S. Lee, and J.E. Kerwin. A B-spline based higher order panel method for analysis of steady flow around marine propellers. Ocean Engineering, 2007, (34), 2045–2060.

[6] Raad Shehab Ahmed. Aerodynamic Parameters Analysis of Transonic Flow Past Unswept and Swept Wings, Eng. & Tech. Journal, Vol. 29, No.5, 2011.

[7] G.K.Ananda, P.P.Sukumar & M.S.Selig. Measured aerodynamic characteristics of wings at low Reynolds numbers. Aerospace Science and Technology, 2015, 42, 392-406.

[8] P. O. Persson1, D. J. Willis, and J. Peraire. Numerical Simulation of Flapping Wings using a Panel Method and a High-Order Navier-Stokes Solver. Int. J. Numer. Meth. Engng, 2011, 01, 1-20.

[9] Joseph Katz Allen Plotkin. LOW SPEED AERODYNAMICS FROM WING THEORY TO PANEL METHODS, international edition 1991, ISBN 0-07-100876-4.

Wakkas Ali Rasheed is Asst. lect. at mechanical Engineering department, College of Engineering, Kufa university. He obtained B.Sc. in mechanical engineering from college of engineering a Kufa university, Iraq 1999 & M.Sc. in mechanical Engineering from the same college in 2002. His reaches interest directed mainly in fields Aerodynamic, (panel method, trojecting of projectiles, air conditioning simulation).
E-mail address: waqas.alibraheemi@uokufa.edu.iq

Nabeel Abdulhadi Ghyadh is Asst. Lect. at Mechanical Engineering Department, College of Engineering, Al-kufa University. He obtained M.Sc. in Mechanical Engineering from College of Engineering, Babylon University, Iraq. (2010) and B.Sc. in Mechanical Engineering from College of Engineering, Al-kufa University, Iraq. (2007). He has published four research papers in reputed International journals and conferences. His research interest is in the field of heat transfer, internal combustion engines and renewable energy.
E-mail address: nabeel.ghayadh@uokufa.edu.iq

Sahib Shehab Ahmed is Asst. Lect. at Mechanical Engineering Department, College of Engineering, Al-kufa University. He obtained M.Sc. in Mechanical Engineering from College of Engineering, Babylon University, Iraq. (2009) and B.Sc. in Mechanical Engineering from College of Engineering, Al-kufa University, Iraq. (2006). He has published three research papers in reputed International journals and conferences. His research interest is in the field of heat transfer, internal combustion engines, aerodynamic and renewable energy.
E-mail address: sahib.aldulaimi@uokufa.edu.iq

